

# SPDEBench: An Extensive Benchmark for Learning Regular and Singular Stochastic PDEs

Zheyang Li <sup>\*</sup>    Yuantu Zhu <sup>†</sup>    Hao Ni <sup>‡</sup>    Siran Li <sup>§</sup>    Bingguang Chen <sup>¶</sup>  
 Qi Meng <sup>||</sup>

May 27, 2025

## Abstract

Stochastic Partial Differential Equations (SPDEs) driven by random noise play a central role in modelling physical processes whose spatio-temporal dynamics can be rough, such as turbulence flows, superconductors, and quantum dynamics. To efficiently model these processes and make predictions, machine learning (ML)-based surrogate models are proposed, with their network architectures incorporating the spatio-temporal roughness in their design. However, it lacks an extensive and unified datasets for SPDE learning; especially, existing datasets do not account for the computational error introduced by noise sampling and the necessary renormalization required for handling singular SPDEs. We thus introduce SPDEBench, which is designed to solve typical SPDEs of physical significance (*e.g.*, the  $\Phi_d^4$ , wave, incompressible Navier–Stokes, and KdV equations) on 1D or 2D tori driven by white noise via ML methods. New datasets for singular SPDEs based on the renormalization process have been constructed, and novel ML models achieving the best results to date have been proposed. In particular, we investigate the impact of computational error introduced by noise sampling and renormalization on the performance comparison of ML models and highlight the importance of selecting high-quality test data for accurate evaluation. Results are benchmarked with traditional numerical solvers and ML-based models, including FNO, NSPDE and DLR-Net, etc. It is shown that, for singular SPDEs, naively applying ML models on data without specifying the numerical schemes can lead to significant errors and misleading conclusions. Our SPDEBench provides an open-source codebase that ensures full reproducibility of benchmarking across a variety of SPDE datasets while offering the flexibility to incorporate new datasets and machine learning baselines, making it a valuable resource for the community. The code is available at [https://github.com/DeepIntoStreams/SPDE\\_hackathon](https://github.com/DeepIntoStreams/SPDE_hackathon).

## 1 Introduction

Stochastic Partial Differential Equations (SPDEs) driven by random noise are important mathematical models for physical processes such as turbulence flows, superconductors, and quantum

<sup>\*</sup>Independent Researcher. Email: [20300180139@fudan.edu.cn](mailto:20300180139@fudan.edu.cn)

<sup>†</sup>School of Mathematical Sciences, Shanghai Jiaotong University. Email: [radonzhu@sjtu.edu.cn](mailto:radonzhu@sjtu.edu.cn)

<sup>‡</sup>Department of Mathematics, University College London. Email: [h.ni@ucl.ac.uk](mailto:h.ni@ucl.ac.uk)

<sup>§</sup>School of Mathematical Sciences, Shanghai Jiaotong University. Email: [siran.li@sjtu.edu.cn](mailto:siran.li@sjtu.edu.cn)

<sup>¶</sup>College of Mathematics and Statistics, Fujian Normal University. Email: [bgchen@fjnu.edu.cn](mailto:bgchen@fjnu.edu.cn)

<sup>||</sup>Academy of Mathematics and Systems Science, Chinese Academy of Sciences. Email: [meq@amss.ac.cn](mailto:meq@amss.ac.cn)

dynamics [7, 8, 10]. SPDEs are both of physical significance and have triggered notable breakthroughs in theoretical mathematics. For example, one major breakthrough in the analysis of SPDEs in the recent decade is Fields Medal work – M. Hairer’s theory of regularity structures [8]. The application of SPDE learning, which means the use of machine learning (ML) models to approximate the dynamics of SPDE, also attracts a lot of attention [2, 16, 4, 15]. One promising framework involves modelling the temporal evolution of time-varying parametric SPDEs via deep neural networks: the neural network learns a mapping from input functions (*e.g.*, initial conditions) to the corresponding solutions [4, 16, 11]. On the practical aspects, the ML-based models such as Neural SPDE [16] and DLR-Net [4] can not only accelerate future state prediction of certain SPDE, but also lead to novel network architectures for modelling spatio-temporal dynamics, which better incorporates the physics prior.

Despite the importance of SPDEs, the field of machine learning SPDEs is still far from being fully explored. First, existing datasets for learning SPDEs are limited, and numerical simulation of SPDEs is highly specialized, and the lack of off-the-shelf software for carrying out such simulations often makes it difficult for researchers to get started. For example, in the theory of regularity structures [7], solutions for singular SPDEs are obtained via delicate renormalization approach (*i.e.*, first considering a sequence of regularized problems driven by mollifications (*i.e.*, the natural smoothing) of the singular noise  $\xi$ , and then subtracting a large constants (“infinities”) from the regularized solutions), but it lacks corresponding datasets for learning singular SPDEs with renormalization. Second, the investigation of ML-based models for learning SPDE overlook important evaluation metrics and coefficients, *e.g.*, the approximation error caused by renormalization, the stability with respect to the noise-truncation degree, which are important in theoretical study of computational SPDEs [12]. Neglecting these metrics can lead to biased and incomplete evaluations of the ML-models.

In view of the above situation, we propose a unified extensible benchmark for studying ML-based models for SPDEs, to promote significant technical advance in designing effective and robust ML-based models to solve physically relevant singular SPDEs (*e.g.*, the  $\Phi_d^4$ , wave, incompressible Navier–Stokes, and KdV equations). We introduce **SPDEBench**, the first extensive benchmark for learning SPDEs which includes API to numerically generate solutions of various SPDEs, pre-generated ready-to-use datasets which cover well-known singular and nonsingular SPDEs, multiple evaluation metrics for training and comparing the machine models, as well as evaluation results of ML models like FNO [11], NSPDE and DLR-Net for learning SPDEs.

SPDEBench has the following distinct features: (a) it takes into consideration the approximation error in the numerical computation of random noise, as well as the renormalization procedure, which allows data generation under various settings of noise truncation degree or renormalization parameters in a user-friendly way; (b) it evaluates the accuracy and robustness for existing machine learning models on the SPDEs under two different noise generation approaches and various settings of the renormalization parameter  $\epsilon$ ; (c) it encompasses a newly designed network architecture by introducing  $\epsilon$  into the input of the neural networks and evaluate its performance on the singular SPDEs. Furthermore, we also discover that the accuracy of most of the ML models decreases as the SPDEs become increasingly singular; among all the tested models, DLR-Net achieves the highest accuracy and is the most robust for learning singular SPDEs. These experimental results shed new lights on the behaviours of ML-learned solutions for SPDEs.

## 2 Preliminaries

In this section, we introduce the fundamental concepts of SPDEs and outline the general formulation for SPDE learning tasks.

### 2.1 Mild solution of SPDE

We consider SPDEs of the form:

$$\begin{aligned}\partial_t u - \mathcal{L}u &= \mu(u, \partial_1 u, \dots, \partial_d u) + \sigma(u, \partial_1 u, \dots, \partial_d u) \xi & \text{in } [0, T] \times D, \\ u(0, x) &= u_0(x),\end{aligned}\tag{1}$$

where  $x \in D \subset \mathbb{R}^d$ ,  $t \in [0, T]$ ,  $\partial_i := \partial/\partial x_i$ ,  $i \in \{1, \dots, d\}$ ,  $\mathcal{L}$  is a linear differential operator,  $\xi : [0, T] \times D \rightarrow \mathbb{R}$  is the stochastic forcing,  $u_0 : D \rightarrow \mathbb{R}$  is the initial datum, and  $\mu, \sigma : \mathbb{R} \times \mathbb{R}^d \rightarrow \mathbb{R}$  are given functions. Under suitable conditions on  $\mu, \sigma$  (e.g., locally Lipschitz), this SPDE has a unique *mild solution* representable via the operator semigroup  $\{e^{t\mathcal{L}}\}$  [7, 16]:

$$u_t = e^{t\mathcal{L}}u_0 + \int_0^t e^{(t-s)\mathcal{L}}\mu(u_s, \partial_1 u_s, \dots, \partial_d u_s) ds + \int_0^t e^{(t-s)\mathcal{L}}\sigma(u_s, \partial_1 u_s, \dots, \partial_d u_s)\xi(ds),$$

where  $u_t(\cdot) := u(t, \cdot)$ ;  $t \in [0, T]$ . In general, if  $\xi$  is function-valued noise, SPDEs have poor regularity in time, and if  $\xi$  is space-time white noise, SPDEs have singularity in space. Throughout this paper, we denote the space-time white noise by  $\xi = \xi(t, x)$  for most equations. It is highly irregular: for parabolic equations it lies in the negative order Hölder space  $\mathcal{C}^{-\frac{d+2}{2}-}$  in spatial dimension  $d = 1, 2, 3, \dots$  [6, 7]. Formal definition of space-time white noise can be found in Supplementary.

### 2.2 Cylindrical Wiener process

Most of the interesting SPDEs do not admit explicit analytical solutions, so the study of computational SPDEs is of great practical and theoretical importance [12]. The deterministic part of SPDEs can be discretized or approximated through traditional numerical methods; e.g., finite difference/finite element methods. Thus, in the sequel we focus on the computation of the stochastic forcing  $\xi$ . In all SPDEs in this benchmark except Navier-Stokes,  $\xi$  is the space-time white noise, which is equivalent to the time derivative of the cylindrical Wiener process.

**Definition 2.1.** [3][Cylindrical Wiener process] Let  $H$  be a separable Hilbert space. A cylindrical Wiener process is the following  $H$ -valued stochastic process:  $W(t) = \sum_{j=1}^{\infty} \phi_j \beta_j(t)$ ,  $t \geq 0$ , where  $\{\phi_j\}$  is any orthonormal basis (ONB) for  $H$  and  $\beta_j(t)$  are i.i.d. Brownian motions.

In theory, the space-time white noise is highly irregular, as  $W$  actually converges in a function space larger than  $H$ . For detailed discussions, we refer the reader to [3], where the technical intricacies are addressed and are thus omitted here.

In 1D case, we set the spatial domain  $D = (0, L)$  and consider an  $L^2(D)$ -valued cylindrical Wiener process  $W(t)$ . We take the ONB  $\phi_k(x) = \sqrt{2/L} \sin(k\pi x/L)$  and sample from the truncated expansion with degree  $J$ , i.e.,  $W^J(t) = \sum_{j=1}^J \phi_j \beta_j(t)$  at the points  $x_m = mL/N$  for  $m = 1, \dots, N$ . In 2D case, we set  $D = (0, L_x) \times (0, L_y)$ , take the  $L^2(D)$ -ONB  $\phi_{j,k}(x, y) = \sqrt{4/L_x L_y} \sin(j\pi x/L_x) \sin(k\pi y/L_y)$ , and sample from the truncations  $W^{J_x, J_y}(t) = \sum_{j=1}^{J_x} \sum_{k=1}^{J_y} \phi_{j,k} \beta_{j,k}(t)$  at  $x_m = mL_x/N_x$ ,  $y_n = nL_y/N_y$  for  $m = 1, \dots, N_x$ ;  $n = 1, \dots, N_y$ .

Cylindrical Wiener process can be regarded as a special case of Q-Wiener process (see details in section 1.2 in Supplementary). For convenience, in what follows we shall use the cylindrical Wiener process to demonstrate the space-time white noise unless mentioned.

### 2.3 Formulation of the learning problem

The objective of machine learning (ML) tasks for SPDE is to find some ML-based surrogate to approximate the mild solution  $u_T(x)$  of the SPDEs. The solution depends not only on the previous time steps of the solution, but also on the random forcing. As this work mainly focused on how the singularity with respect to the space-time white noise and renormalization influence the learning, the learning target is to approximate the following operators:

- $\mathcal{G}_1 : \xi(x) \rightarrow u_T(x)$  under fixed initial datum  $u_0(x)$ ;
- $\mathcal{G}_2 : (u_0(x), \xi(x)) \rightarrow u_T(x)$  where  $u_0(x)$  follows a given distribution.

In practice, the spatial domain  $D$  gets discretized into meshes and  $u_T(x)$  is approximated by numerical methods. The target now becomes approximating the following operators using ML-based surrogates:

- $\hat{\mathcal{G}}_1 : \xi(x) \rightarrow \hat{u}_T(x)$  under fixed initial condition  $u_0(x)$ ;
- $\hat{\mathcal{G}}_2 : (u_0(x), \hat{\xi}(x)) \rightarrow \hat{u}_T(x)$  where  $u_0(x)$  follows a given distribution.

Here,  $x$  belongs to a discretized mesh,  $\hat{\xi}$  is sampled by the cylindrical Wiener process with truncation degree  $J$ , and  $\hat{u}_T(x)$  is generated by numerical solvers. Given a dataset  $\mathcal{Z} = \left\{ \left( \hat{\xi}^{(i)}, \hat{u}_T^{(i)} \right) \mid i = 1, \dots, n; u_0; J \right\}$  or  $\mathcal{Z} = \left\{ \left( u_0^{(i)}, \hat{\xi}^{(i)}; \hat{u}_T^{(i)} \right) \mid i = 1, \dots, n; u_0 \right\}$ , the ML-based models, e.g., the neural network  $f_w$  with parameters  $w$ , are optimized via the optimization problem:

$$f^* = \arg \min_w \frac{1}{n} \sum_{i=1}^n L \left( f_w(\hat{\xi}^{(i)}, \hat{u}_0^{(i)}) - \hat{u}_T^{(i)} \right), \quad (2)$$

where  $L(\cdot, \cdot)$  denotes the loss function.

## 3 SPDEBench: A Benchmark for Learning SPDEs

In the following, we describe the details of SPDEBench, including the overview of datasets, existing implemented ML models developed using PyTorch, and implementation guidance for users.

### 3.1 Overview of Datasets

We are primarily concerned with developing ML-based approaches to solving SPDEs, which are of considerable significance in theoretical and applied sciences. Many important physically relevant SPDEs fall into this category, and in the SPDEBench, we generate two classes of the datasets: the nonsingular SPDE datasets and a novel singular SPDE dataset. The key information of the SPDEs in SPDEBench is summarized in Table 1 and Table 2.

Table 1: SPDEs with their respective spatial domain  $D$ , time interval  $[0, T]$ , spatial resolution  $N_D$ , temporal resolution  $N_t$ , numbers of selected truncation degree  $N_J$  and number of generated samples  $N_Z$  for each degree. The rightarrow  $n \rightarrow m$  means the resolution is downsampled from  $n$  to  $m$ .

| SPDE                     | Space      | Time         | $N_D$                   | $N_t$                  | $N_J$ | $N_Z$ |
|--------------------------|------------|--------------|-------------------------|------------------------|-------|-------|
| Ginzburg–Landau          | $[0, 1]$   | $[0, 0.05]$  | 128                     | 50                     | 4     | 1200  |
| Korteweg–De Vries (KdV)  | $[0, 1]$   | $[0, 0.5]$   | 128                     | 50                     | 4     | 1200  |
| Wave                     | $[0, 1]$   | $[0, 0.5]$   | 128                     | $500 \rightarrow 100$  | 4     | 1200  |
| Incompressible NSE       | $[0, 1]^2$ | $[0, 1]$     | $64^2 \rightarrow 16^2$ | $1000 \rightarrow 100$ | 4     | 1200  |
| Dynamic $\Phi_2^4$ Model | $[0, 1]^2$ | $[0, 0.025]$ | $32 \times 32$          | 250                    | 4     | 1200  |

Table 2: The noise type, truncation degree  $J$  and with/without renormalization for generating datasets.

| SPDE                     | Noise type                 | $J$                     | Renormalization |
|--------------------------|----------------------------|-------------------------|-----------------|
| Ginzburg–Landau          | cylindrical Wiener process | $\{32, 64, 128, 256\}$  | No              |
| Korteweg–De Vries (KdV)  | cylindrical Wiener process | $\{32, 64, 128, 256\}$  | No              |
| Wave                     | cylindrical Wiener process | $\{32, 64, 128, 256\}$  | No              |
| Incompressible NSE       | Q-Wiener process           | $\{32, 64, 128, 256\}$  | No              |
| Dynamic $\Phi_2^4$ Model | cylindrical Wiener process | $\{2, 8, 32, 64, 128\}$ | Yes             |

### 3.1.1 Nonsingular SPDE datasets

The nonsingular SPDE datasets include 1D Ginzburg–Landau equation, 1D Korteweg–De Vries (KdV) equation, 1D wave equation and the 2D incompressible Navier–Stokes equation (NSE, in the form of vorticity equation). For each equation with one noise truncation degree, we generate 1200 samples. We define the 1D torus  $\mathbf{T}^1 = \mathbb{R}/\mathbb{Z}$  by identifying the endpoints of the interval  $[0, 1]$ , and the 2D torus  $\mathbf{T}^2$  is obtained by identifying the opposite sides of the square  $[0, 1]^2$  in the following context. We next introduce the details for data generation in these datasets.

**Ginzburg–Landau Equation.** Consider the Ginzburg–Landau equation:

$$\begin{cases} \partial_t u - \Delta u = 3u - u^3 + \sigma \xi & \text{in } [0, 0.05] \times \mathbf{T}^1, \\ u|_{t=0} = u_0 & \text{at } \{0\} \times \mathbf{T}^1. \end{cases}$$

Following the setup in previous work [16], we set the initial condition as  $u_0(x) = x(1 - x) + \kappa\eta(x)$  with  $\eta(x) = \sum_{k=-10}^{k=10} \frac{a_k}{(|k|+1)^2} \sin(2k\pi x)$ , where  $a_k \stackrel{\text{i.i.d.}}{\sim} \mathcal{N}(0, 1)$ . We take  $\kappa = 0$  or  $\kappa = 0.1$  to generate datasets with fixed or varying initial conditions, respectively. We use finite difference method to solve the SPDE. The space-time white noise is sampled from the truncated cylindrical Wiener process and scaled by  $\sigma = 1$ .

**Korteweg–De Vries (KdV) Equation.** Consider the KdV Equation for shallow water:

$$\begin{cases} \partial_t u - 0.001\partial_{xx}u + \gamma\partial_{xxx}u = 6u\partial_x u + \sigma \xi & \text{in } [0, 0.5] \times \mathbf{T}^1, \\ u|_{t=0} = u_0 & \text{at } \{0\} \times \mathbf{T}^1. \end{cases}$$

In our experiments, we take  $\gamma = 0.1$ . The initial datum is  $u_0(x) = \sin(2\pi x) + \kappa\eta(x)$ , where  $\eta$  is defined as for the Ginzburg–Landau Equation. Similarly, we take  $\kappa = 0$  or  $\kappa = 0.1$  to

generate datasets with fixed or varying initial conditions, respectively. The numerical solution was calculated using the spectral Galerkin method. The space-time white noise is sampled from the truncated cylindrical Wiener process and scaled by  $\sigma = 0.5$ .

**Wave Equation.** Consider the wave Equation:

$$\begin{cases} \partial_{tt}u - \partial_{xx}u = \cos(\pi u) + u^2 + u \cdot \xi & \text{in } [0, 0.5] \times \mathbf{T}^1, \\ (u, \partial_t u)|_{t=0}(x) = (u_0(x), v_0(x)) & \text{at } \{0\} \times \mathbf{T}^1. \end{cases}$$

We set  $u_0(x) = \sin(2\pi x) + \kappa\eta(x)$  and  $v_0(x) = x(1-x)$ , where  $\eta(x)$  is as before and  $\kappa$  is set to be 0 or 0.1. The numerical solution was calculated with both temporally and spatially 2nd-order central difference scheme. The space-time white noise is sampled from truncated cylindrical Wiener process.

**Incompressible Navier–Stokes equation.** In our competition, we consider the (scalar) *vorticity equation* on the 2D torus, obtained by taking the curl of the Navier–Stokes Equation:

$$\begin{cases} \partial_t \omega - \nu \Delta \omega = -u \cdot \nabla \omega + f + \sigma \xi & \text{in } [0, 1] \times \mathbf{T}^2, \\ \omega|_{t=0} = \omega_0 & \text{at } \{0\} \times \mathbf{T}^2. \end{cases}$$

Here, the velocity field  $u = [u^1, u^2]^\top$  is incompressible ( $\text{div } u = 0$ ), and the vorticity is defined as  $\omega = \text{curl } u = [\partial_2 u^1, -\partial_1 u^2]^\top$ . In experiments, we take the coefficients  $\nu = 10^{-4}$ ,  $\sigma = 0.005$ , and  $f = 0.1(\sin(2\pi(x+y)) + \cos(2\pi(x+y)))$  [11]. The initial condition is generated according to  $\omega_0 \sim \mu$ , where  $\mu = \mathcal{N}(0, 3^{3/2}(-\Delta + 9I)^{-3})$ . The numerical solution was calculated using the spectral Galerkin method. The colored-in-space noise is the sum of 10 trajectories sampled from truncated Q-Wiener process.

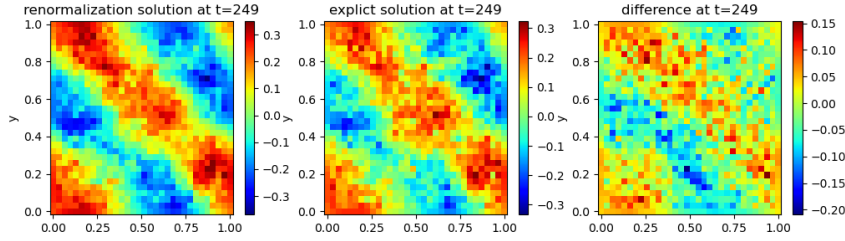


Figure 1: Comparison of two data generation methods of  $\Phi_2^4$  when truncation degree  $J = 128$  at time step  $t = 249$ . The left panel is mean of 1200 samples generated through the renormalization procedure, while the right panel is mean of 1200 samples generated through an explicit scheme without implementing the renormalization.

### 3.1.2 A novel singular SPDE dataset

**The dynamical  $\Phi_2^4$  model.** Consider the dynamical  $\Phi_2^4$  model:

$$\begin{cases} \partial_t u = \Delta u - u^3 + \sigma \xi & \text{in } [0, T] \times \mathbf{T}^2, \\ u|_{t=0} = u_0 & \text{at } \{0\} \times \mathbf{T}^2. \end{cases}$$

We set the initial condition as  $u_0(x, y) = \sin(2\pi(x+y)) + \cos(2\pi(x+y)) + \kappa\eta(x, y)$  with  $\eta(x, y) = a_0 + \sum_{j=-10}^{j=10} \sum_{k=-10}^{k=10} \frac{a_{j,k}}{|j|^2 + |k|^2 + 1} \sin((j\pi x - k\pi y)/2)$ , where  $a_0, a_{j,k} \stackrel{\text{i.i.d.}}{\sim} \mathcal{N}(0, 1)$ . The

numerical solution is calculated with the temporally 1st order and spatially 2nd order difference scheme. The space-time white noise is sampled from the truncated cylindrical Wiener process and scaled by  $\sigma = 0.1$ . In this case, the nonlinear term  $u^3$  is undefined in classical sense (see details in A.3 in Supplementary). Its rigorous definition requires the renormalization procedure, which shall be implemented in this work via the following:

**Wick power of stochastic convolution.** Consider the stochastic convolution  $X$ :

$$\partial_t X - \Delta X = \xi, \quad X(0) = u_0.$$

We start by replacing  $\xi$  with a suitable mollification  $\xi_\varepsilon = \xi * \eta_\varepsilon$  (where  $\eta_\varepsilon$  stands for a smoothing kernel). For  $\xi$  generated via a cylindrical Wiener process, the mollification is equivalent to the Galerkin approximation. For notational convenience, we rewrite the stochastic convolution with truncated Galerkin projection and solve for  $X_\varepsilon := X_{J-1}$  from  $dX_{J-1} - \Delta X_{J-1} dt = dW^J(t)$ .

The *Wick power* of  $X$ , denoted as  $X^{\diamond n}$  ( $n = 2, 3$ ), is defined as

$$X^{\diamond 2} := \lim_{J \rightarrow \infty} (X_{J-1}^2 - a_{J-1}), \quad X^{\diamond 3} := \lim_{J \rightarrow \infty} (X_{J-1}^3 - 3a_{J-1}X_{J-1}),$$

with  $a_\varepsilon := a_{J-1} = \mathbb{E}[X_{J-1}^2]$  (See [5] for details). Now we substitute the ansatz  $u(t) = X(t) + v(t)$  into the dynamical  $\Phi_2^4$  model, with  $X$  is the stochastic convolution above. Then  $v$  satisfies the shift equation:  $dv = \Delta v dt - u^3 dt, v(0) = 0$ , where  $u^3$  should be interpreted as the renormalization term  $u^{\diamond 3}$  given by the Wick powers of  $X$ :  $u^{\diamond 3} \equiv v^3 + 3v^2X + 3vX^{\diamond 2} + X^{\diamond 3}$ . The renormalized equation is now well-defined for any  $\alpha > 0$ :

$$\partial_t u - \Delta u + u^{\diamond 3} = \xi, \quad u(0) = u_0. \quad (3)$$

Figure 1 shows the comparison of two data generation method of  $\Phi_2^4$  when truncation degree  $J = 128$ . It shows that the solution generated without implementing renormalization is more noisy in space while the solution generated through renormalization has clearer pattern.

### 3.2 Baseline ML Surrogate Models

SPDEBench implements several network architectures as surrogate models for practical use and comparative analysis. SPDEBench includes the following existing baseline models and also a modified model for learning singular SPDE.

**NCDE, NRDE and NCDE-FNO** These three rough path theory-inspired ML models [9, 14, 16] incorporate the signatures of controlled differential equations into the network architecture design. They are particularly suitable for irregularly sampled time-series data, allowing for adaptive computation and memory-efficient training.

**FNO and DeepONet** Fourier neural operator [11] and DeepONet [13] are two representative Neural Operators designed for approximating solutions of parametric PDEs. They are capable of modelling maps between function spaces, which serve as generalizations for classical neural networks.

**NSPDE** Taking spatial-temporal randomness into account, Salvi *et al* [16] introduced neural SPDE (NSPDE), a neural operator architecture for modelling operators in SPDEs that take both the initial data and stochastic forcing as inputs.

**DLR-Net** The Deep Latent Regularity Network (DLR-Net) [4] is a neural architecture combining the regularity feature in the theory of regularity structures with deep neural network, making it particularly robust for SPDE learning whose solution may be rough both temporally and spatially.

**NSPDE-S** We extend the NSPDE model by adding one input channel for the parameter  $\epsilon$  in the renormalization for learning singular SPDEs with renormalization.

```

from huggingface_hub import hf_hub_download
import pandas as pd

REPO_ID = ""
FILENAME = ""

dataset = pd.read_csv(
    hf_hub_download(repo_id=REPO_ID, filename=FILENAME, repo_type="dataset")
)

```

Listing 1: Including a benchmark dataset

### 3.3 Data Format, Benchmark Access, Maintenance, and Extensibility

The benchmark comprises multiple data files in Parquet format, each corresponding to a specific combination of equation, initial condition type, noise type, truncation degree of the driving noise, and data generation method. Each file contains multiple one-dimensional arrays of length  $N \times T \times X \times Y$ , generated by flattening arrays with dimensions  $N, T, X, Y$  with  $N$  the number of samples,  $T$  the number of time steps, and  $X, Y$  the spatial dimensions. More information on the data format is provided in Supplementary Materials.

SPDEBench’s datasets are stored and maintained using Hugging Face ([https://huggingface.co/datasets/SSPDEBench/Reuglar\\_and\\_Singular\\_SPDEBench](https://huggingface.co/datasets/SSPDEBench/Reuglar_and_Singular_SPDEBench)). Through Hugging Face, we provide a permanent DOI (doi:10.57967/hf/5500) for the benchmark data. A dedicated team ensures that the benchmark is continuously maintained. We also support a straightforward inclusion of the benchmark with a few lines of code. In Listing 1, we demonstrate the way in which the Hugging Face platform supports the integration of pre-generated datasets using a few lines of code.

Examples that leverage pre-defined classes in our benchmark code to load specific datasets as PyTorch Dataset objects are provided in section B in Supplementary. Subsequently, these can be used to construct common DataLoader instances for training the ML models. While our implementation of SPDEBench builds upon the GitHub repositories of Neural SPDE (<https://github.com/crispitaagorico/torchspde>) [16] and DLR-Net (<https://github.com/sdogsq/DLR-Net>) [4], it significantly extends them by providing a unified and modular benchmarking framework that supports a broader range of ML-based surrogate SPDE models for comprehensive evaluation. It should be noted that, to construct the Parquet-formatted data, all data have been flattened into 1D arrays. When accessing the data, users will need to reshape these arrays back to their original dimensions. We provide detailed code for this process in section B in Supplementary for reference.

## 4 Experiments

In this section, we present a selection of experiments on the SPDEBench datasets. An extensive set of additional results and details on hyper-parameters can be found in the Supplementary Materials. In all the experiments, both the loss function and testing metric are selected as the relative  $L^2$ -error [16].

#### 4.1 The effect of renormalization on accuracy

We use the singular dataset  $\Phi_2^4$  to study the effect of renormalization on the performance of the ML-based models. Denote by  $\mathcal{D}_J^{\text{re}}$  and  $\mathcal{D}_J$  the datasets constructed with and without renormalization, respectively. Both involve truncating the noise up to degree  $J$ . For each dataset  $\mathcal{D}_J$  or  $\mathcal{D}_J^{\text{re}}$ , we use its training dataset to train the NSPDE model and evaluate it on the corresponding test dataset. We also evaluate it on the test dataset of  $\mathcal{D}_{J_{\max}}^{\text{re}}$  as the proxy of ground truth. Moreover, we use NSPDE-S to learn the functional relations between the input  $J$  (or the corresponding renormalization constant  $a_\epsilon$ , which is defined in section 3.1.2) and  $\xi$  (or  $\mu_0, \xi$ ) and the output  $u$  on the dataset composing of the dataset  $\mathcal{D}^{\text{re}} = \bigcup_J \mathcal{D}_J^{\text{re}}$  and report the performance on  $\mathcal{D}_{J_{\max}}^{\text{re}}$ .

Table 3: Relative  $L^2$ -error on the test set of the dynamical  $\Phi_2^4$  model. Data are generated by implementing the renormalization method.

| Task                            | $\xi \mapsto u$                      |                                      | $(\xi, a_\epsilon) \mapsto u$ |                                      | $(\xi, u_0) \mapsto u$               |                                      | $(\xi, u_0, a_\epsilon) \mapsto u$ |                                      |
|---------------------------------|--------------------------------------|--------------------------------------|-------------------------------|--------------------------------------|--------------------------------------|--------------------------------------|------------------------------------|--------------------------------------|
| Train set/Test set              | $\mathcal{D}_J^{\text{re}}$          | $\mathcal{D}_{J_{\max}}^{\text{re}}$ | $\mathcal{D}_J^{\text{re}}$   | $\mathcal{D}_{J_{\max}}^{\text{re}}$ | $\mathcal{D}_J^{\text{re}}$          | $\mathcal{D}_{J_{\max}}^{\text{re}}$ | $\mathcal{D}_J^{\text{re}}$        | $\mathcal{D}_{J_{\max}}^{\text{re}}$ |
| $\mathcal{D}_2^{\text{re}}$     | 0.010                                | 4.087                                | 0.034                         | 0.998                                | 0.010                                | 2.805                                | 0.042                              | 0.998                                |
| $\mathcal{D}_8^{\text{re}}$     | 0.012                                | 1.720                                | 0.012                         | 0.977                                | 0.017                                | 1.318                                | 0.014                              | 0.977                                |
| $\mathcal{D}_{32}^{\text{re}}$  | 0.051                                | 1.145                                | 0.034                         | 0.947                                | 0.052                                | 1.180                                | 0.028                              | 0.947                                |
| $\mathcal{D}_{64}^{\text{re}}$  | 0.117                                | 0.722                                | 0.031                         | 0.754                                | 0.112                                | 0.475                                | 0.023                              | 0.755                                |
| $\mathcal{D}_{128}^{\text{re}}$ | 0.230                                | 0.230                                | 0.028                         | 0.028                                | 0.223                                | 0.223                                | 0.029                              | 0.029                                |
| Task                            | $(\xi, a_\epsilon) \mapsto u$        |                                      |                               |                                      | $(\xi, u_0, a_\epsilon) \mapsto u$   |                                      |                                    |                                      |
| Train set/Test set              | $\mathcal{D}_{J_{\max}}^{\text{re}}$ |                                      |                               |                                      | $\mathcal{D}_{J_{\max}}^{\text{re}}$ |                                      |                                    |                                      |
| $\mathcal{D}^{\text{re}}$       | 0.231                                |                                      |                               |                                      | 0.291                                |                                      |                                    |                                      |

The experimental results are reported in Table 3. As the noise truncation degree  $J$  increases from 2 to 128, the performance of NSPDE worsens while NSPDE-S performs more consistently. It indicates that applying ML models on data with specified numerical schemes is necessary for achieving accurate results and NSPDE-S with the renormalization constant as input significantly helps the performance.

We also conduct experiments for the  $\Phi_2^4$  equation on the data generated without implementing the renormalization (denote by  $\mathcal{D}_J^{\text{ex}}$  the corresponding datasets). We train NSPDE model similarly as it is trained under the renormalization setting, and we report the performance in Table 4. Comparing the results in Table 3 and Table 4, we can conclude that renormalization helps learning and reduces the relative  $L^2$ -error on  $\mathcal{D}_J$  but increases the approximation error  $\mathcal{D}_{J_{\max}}$ . The results reflect how and to what extent the regularity and renormalization effects the performance of the learning task.

Table 4: Relative  $L^2$ -error on the test set of the  $\Phi_2^4$  model. Data are generated without the renormalization method.

| Task                            | $\xi \mapsto u$             |                                      | $(\xi, u_0) \mapsto u$      |                                      |
|---------------------------------|-----------------------------|--------------------------------------|-----------------------------|--------------------------------------|
| Train set/Test set              | $\mathcal{D}_J^{\text{ex}}$ | $\mathcal{D}_{J_{\max}}^{\text{re}}$ | $\mathcal{D}_J^{\text{ex}}$ | $\mathcal{D}_{J_{\max}}^{\text{re}}$ |
| $\mathcal{D}_2^{\text{ex}}$     | 0.009                       | 3.206                                | 0.010                       | 3.135                                |
| $\mathcal{D}_8^{\text{ex}}$     | 0.016                       | 0.902                                | 0.016                       | 1.412                                |
| $\mathcal{D}_{32}^{\text{ex}}$  | 0.075                       | 1.220                                | 0.070                       | 1.187                                |
| $\mathcal{D}_{64}^{\text{ex}}$  | 0.139                       | 0.447                                | 0.138                       | 0.422                                |
| $\mathcal{D}_{128}^{\text{ex}}$ | 0.261                       | 0.226                                | 0.260                       | 0.224                                |

Table 5: Inference time on  $\Phi_2^4$ .

| Model         | #Para   | Time (ms) |
|---------------|---------|-----------|
| Solver (Reno) | x       | 129.291   |
| Solver (Expl) | x       | 103.770   |
| FNO           | 395145  | 0.572     |
| NSPDE         | 2103809 | 0.471     |
| NSPDE-S       | 2103809 | 0.479     |

## 4.2 The effect of noise simulation on accuracy

In this section, we explore the effects of hyper-parameters in the stochastic forcing simulation (*e.g.*, truncation degree, scale parameter, and approximation methods) on the performance of ML-models. We will report the experimental results on several baseline models and datasets, with implementation details included in Supplementary Materials.

### 4.2.1 The effect of noise truncation degree

Table 6 shows the relative  $L^2$ -errors for several models on the Ginzburg–Landau equation, whose space-time white noise is simulated using truncated cylindrical Wiener process with degree  $J = \{32, 64, 128, 256\}$ . The results show that NSPDE and DLR-Net achieve the lowest error. Meanwhile, NSPDE performs better when the truncation degree is lower, while DLR-Net performs better when the truncation degree is higher. We next investigate the performance of the baseline models on the Ginzburg–Landau equation with  $\sigma = 1$ , a larger-scale parameter before the noise term. The results are reported in Table 7. We found that the DLR-Net significantly outperforms the others when  $\sigma = 1$ . Both indicate that the regularity features in DLR-Net can tailor the singularity and help the performance of ML-model for the more singular cases.

We also explore the performance for these baseline models on other datasets such as the KdV equation, wave equation and Navier-Stokes equation, and the results are reported in Supplementary.

Table 6: Relative  $L^2$ -error on the test set of the Ginzburg-Landau ( $\Phi_1^4$ ) Equation. Data is generated with different truncation degree ( $J=32 \mid 64 \mid 128 \mid 256$ ) and  $\sigma = 0.1$ .

| Model            | #Para   | Inference<br>time (ms) | $\xi \mapsto u$ |       |       |       | $(u_0, \xi) \mapsto u$ |       |       |       |
|------------------|---------|------------------------|-----------------|-------|-------|-------|------------------------|-------|-------|-------|
|                  |         |                        | $J = 32$        | $64$  | $128$ | $256$ | $J = 32$               | $64$  | $128$ | $256$ |
| Numerical Solver | x       | 2.438                  | x               |       |       |       | x                      |       |       |       |
| NCDE             | 545088  | 0.197                  | 0.063           | 0.064 | 0.067 | 0.099 | 0.103                  | 0.106 | 0.109 | 0.147 |
| NRDE             | 8656656 | 0.201                  | 0.129           | 0.127 | 0.129 | 0.181 | 0.147                  | 0.145 | 0.144 | 0.204 |
| NCDE-FNO         | 48769   | 1.734                  | 0.031           | 0.040 | 0.054 | 0.070 | 0.032                  | 0.041 | 0.050 | 0.070 |
| DeepONet         | 4329472 | 0.009                  | 0.109           | 0.118 | 0.123 | 0.174 | x                      |       |       |       |
| FNO              | 4924449 | 0.166                  | 0.019           | 0.019 | 0.019 | 0.027 | x                      |       |       |       |
| NSPDE            | 3283457 | 0.156                  | 0.001           | 0.001 | 0.003 | 0.004 | 0.001                  | 0.001 | 0.003 | 0.004 |
| DLR-Net          | 133178  | 0.110                  | 0.003           | 0.001 | 0.002 | 0.001 | 0.002                  | 0.001 | 0.002 | 0.001 |

### 4.2.2 The effect of noise approximation method

In this subsection, we compare the performance for ML models on the datasets with noise generated via truncated cylindrical Wiener and a Q-Wiener processes (see details in Supplementary). Part of the results are shown in Figure 2, which compares the relative  $L^2$ -errors for learning the KdV equation using the above two different noise generation methods for FNO and NSPDE. It shows that different noise generation methods also impact the learning performance.

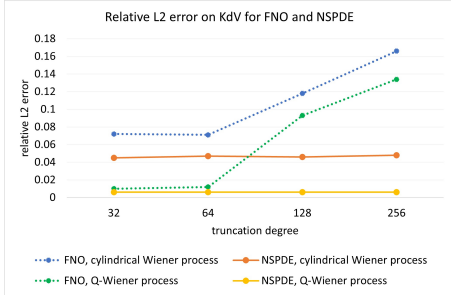
## 4.3 Inference Time Comparison

In this subsection, we compare the per-sample inference time of the numerical solvers with that of ML models. We denote the numerical simulation with renormalization as "Solver (Reno)" and that without implementing the renormalization as "Solver (Expl)" in Table. 5). Timings for the two numerical solvers were recorded on an Intel Xeon Platinum 8352V CPU, whereas the ML

models' inference was measured on a RTX 4090(24GB) GPU with PyTorch@2.4 and CUDA@12.1. Despite the difference in devices, these measurements offer insight into the relative performance of the numerical solvers and ML models. The inference time on  $\Phi_1^4$  and  $\Phi_2^4$  is reported in Table 6 and Table 5 respectively. When timing the numerical solvers, we use the same data resolutions as in the initial data generation (Table 1). When timing the ML models, the resolution of test data is the same as in model training. We measure the average time each ML model takes to perform inference on a batch (batch size = 100) of samples, and then divide it by the batch size to obtain the average inference time per sample. The results show that the ML models significantly improve simulation efficiency.

Table 7: Relative  $L^2$ -error on the test set of the Ginzburg-Landau ( $\Phi_1^4$ ) Equation. Data is generated with different truncation degree ( $J=32 \mid 64 \mid 128 \mid 256$ ) and  $\sigma = 1$ .

| Model    | $\xi \mapsto u$ |       |       |       | $(u_0, \xi) \mapsto u$ |       |       |       |
|----------|-----------------|-------|-------|-------|------------------------|-------|-------|-------|
|          | $J=32$          | $64$  | $128$ | $256$ | $J=32$                 | $64$  | $128$ | $256$ |
| NCDE     | 0.509           | 0.497 | 0.510 | 0.632 | 0.506                  | 0.546 | 0.593 | 0.633 |
| NRDE     | 0.868           | 0.822 | 0.856 | 0.944 | 0.846                  | 0.855 | 0.863 | 0.935 |
| NCDE-FNO | 0.215           | 0.224 | 0.270 | 0.299 | 0.196                  | 0.226 | 0.311 | 0.308 |
| DeepONet | 0.783           | 0.784 | 0.841 | 0.923 | x                      |       |       |       |
| FNO      | 0.132           | 0.126 | 0.135 | 0.148 | x                      |       |       |       |
| NSPDE    | 0.009           | 0.011 | 0.019 | 0.021 | 0.010                  | 0.009 | 0.021 | 0.022 |
| DLR-Net  | 0.002           | 0.001 | 0.003 | 0.001 | 0.001                  | 0.001 | 0.001 | 0.001 |



| Model               | $\xi \mapsto u$ |       |       |       |
|---------------------|-----------------|-------|-------|-------|
|                     | $J=32$          | $64$  | $128$ | $256$ |
| FNO (Q-Wiener)      | 0.045           | 0.047 | 0.046 | 0.048 |
| NSPDE (Q-Wiener)    | 0.006           | 0.006 | 0.006 | 0.006 |
| FNO (cylindrical)   | 0.072           | 0.071 | 0.118 | 0.166 |
| NSPDE (cylindrical) | 0.010           | 0.012 | 0.093 | 0.134 |

Figure 2: Comparison of FNO and NSPDE trained on KdV datasets with noise generated by cylindrical Wiener process ( $\sigma = 0.5$ ) and Q-Wiener process ( $\sigma = 1$ ).

## 5 Conclusions and Limitations

Our work addresses the challenge of modeling and solving SPDEs, which are critical to understanding complex physical systems such as turbulence and quantum dynamics. We introduce SPDEBench, an extensive benchmark for machine learning SPDEs, which includes singular and non-singular SPDE datasets and baseline ML models for evaluation. SPDEBench is among the very first ML implementations of highly irregular SPDEs solutions in the framework of regularity structures. It is expected to shed new light on ML methodologies for SPDEs, especially on the developments of novel designs for AI approaches to the singular SPDEs.

**Limitations:** Our dataset currently emphasizes certain equations with physical significance, potentially underrepresenting others that might be important in different domains. For example, we did not include the hyperbolic SPDEs. We aim to mitigate this by encouraging community contributions and extension of SPDEBench to cover more equation types and parameter regimes.

**Broader impact:** The proposed SPDEBench dataset and ML models will benefit researchers and practitioners in applied mathematics, computational physics, and engineering who rely on efficient surrogates for expensive or intractable numerical simulations. It also supports the machine learning community in developing and benchmarking models capable of capturing spatio-temporal roughness in data, thus facilitating broader advancements in scientific machine learning. To prevent misinterpretation or over-reliance, SPDEBench ensures transparency in data generation and evaluation, especially given the challenges posed by singularities and numerical artifacts.

## References

- [1] H. Bahouri, J.-Y. Chemin, and R. Danchin. Fourier Analysis and Nonlinear Partial Differential Equations. Springer Berlin Heidelberg, 2011.
- [2] I. Chevyrev, A. Gerasimovičs, and H. Weber. Feature engineering with regularity structures. Journal of Scientific Computing, 98(1):13, 2024.
- [3] G. Da Prato and J. Zabczyk. Stochastic equations in infinite dimensions, volume 152. Cambridge university press, 2014.
- [4] S. Gong, P. Hu, Q. Meng, Y. Wang, R. Zhu, B. Chen, Z. Ma, H. Ni, and T.-Y. Liu. Deep latent regularity network for modeling stochastic partial differential equations. In Proceedings of the AAAI Conference on Artificial Intelligence, volume 37, pages 7740–7747, 2023.
- [5] M. Gubinelli and M. Hofmanová. Global solutions to elliptic and parabolic  $\Phi^4$  models in euclidean space. Communications in Mathematical Physics, 368(3):1201–1266, 2019.
- [6] M. Gubinelli, P. Imkeller, and N. Perkowski. Paracontrolled distributions and singular PDEs. In Forum of Mathematics, Pi, volume 3, page e6. Cambridge University Press, 2015.
- [7] M. Hairer. Solving the KPZ equation. Annals of mathematics, pages 559–664, 2013.
- [8] M. Hairer. A theory of regularity structures. Inventiones mathematicae, 198(2):269–504, 2014.
- [9] P. Kidger, J. Morrill, J. Foster, and T. Lyons. Neural controlled differential equations for irregular time series. Advances in neural information processing systems, 33:6696–6707, 2020.
- [10] J. R. Klauder. Stochastic quantization. In Recent developments in high-energy physics, pages 251–281. Springer, 1983.
- [11] Z. Li, N. Kovachki, K. Azizzadenesheli, B. Liu, K. Bhattacharya, A. Stuart, and A. Anandkumar. Fourier neural operator for parametric partial differential equations. arXiv preprint arXiv:2010.08895, 2020.
- [12] G. J. Lord, C. E. Powell, and T. Shardlow. An introduction to computational stochastic PDEs, volume 50. Cambridge University Press, 2014.

- [13] L. Lu, P. Jin, G. Pang, Z. Zhang, and G. E. Karniadakis. Learning nonlinear operators via deeponet based on the universal approximation theorem of operators. Nature machine intelligence, 3(3):218–229, 2021.
- [14] J. Morrill, C. Salvi, P. Kidger, and J. Foster. Neural rough differential equations for long time series. In International Conference on Machine Learning, pages 7829–7838. PMLR, 2021.
- [15] A. Neufeld and P. Schmock. Solving stochastic partial differential equations using neural networks in the wiener chaos expansion. arXiv preprint arXiv:2411.03384, 2024.
- [16] C. Salvi, M. Lemercier, and A. Gerasimovics. Neural stochastic PDEs: Resolution-invariant learning of continuous spatiotemporal dynamics. Advances in Neural Information Processing Systems, 35:1333–1344, 2022.
- [17] H. Triebel. Theory of Function Spaces III, volume 100. Birkhäuser Basel, 2006.

This is the **Supplementary Materials** for "SPDEBench: An Extensive Benchmark for Learning Regular and Singular Stochastic PDEs".

## A Basic Concepts in SPDE Theory

### A.1 Space-time white noise

In most cases, the noise term  $\xi = \xi(t, x)$  is introduced to represent a so-called space-time white noise. Noise of this type can be viewed as a "delta-correlated" random distribution. Formally, a space-time white noise in  $\mathbb{R}^n$  is a Gaussian random variable with mean zero and correlation:

$$\mathbb{E} [\xi(t, x)\xi(s, y)] = \delta(t - s)\delta(x - y),$$

where  $\delta$  denotes the delta function. It, of course, is not an actual function but a distribution, and  $\xi$  should be interpreted as a random distribution. That is,  $\xi$  is a generalized centred Gaussian random field, with covariance defined in the sense of test functions:

$$\mathbb{E} [\langle \xi, h \rangle \langle \xi, k \rangle] = \int_0^T \int_{\mathbb{R}^n} h(t, x)k(t, x) dx dt, \quad \forall h, k \in L^2([0, T] \times \mathbb{R}^n).$$

This is equivalent to the time derivative of the cylindrical Wiener process defined in Section 2.2.

As a slight variant, noise term white in time and "colored" in space can be introduced as

$$\mathbb{E} [\xi(t, x)\xi(s, y)] = \delta(t - s)q(x - y),$$

where  $q$  is the correlation function. The smoother  $q$  is, the more regular is the noise. The colored noise terms can be represented as the time derivative of  $Q$ -Wiener processes in the next subsection.

### A.2 $Q$ -Wiener process

Let  $H$  be a separable Hilbert space with a complete orthonormal basis (ONB)  $\{\phi_k\}_{k \in \mathbb{N}}$ . Consider an operator  $Q \in \mathcal{L}(H)$  such that there exists a bounded sequence of nonnegative real numbers  $\{\lambda_k\}_{k \in \mathbb{N}}$  such that  $Q\phi_k = \lambda_k\phi_k$  for all  $k \in \mathbb{N}$  (this is implied by  $Q$  being a trace class, non-negative, symmetric operator, for example).

**Definition A.1** ( $Q$ -Wiener process). Let  $(\Omega, \mathcal{F}, \mathcal{F}_t, \mathbb{P})$  be a filtered probability space. A  $H$ -valued stochastic process  $\{W(t) : t \geq 0\}$  is a  $Q$ -Wiener process if

1.  $W(0) = 0$  almost surely;
2.  $W(t; \omega)$  is a continuous sample trajectory  $\mathbb{R}^+ \mapsto H$ , for each  $\omega \in \Omega$ ;
3.  $W(t)$  is  $\mathcal{F}_t$ -adapted and  $W(t) - W(s)$  is independent of  $\mathcal{F}_s$  for  $s < t$ ;
4.  $W(t) - W(s) \sim \mathcal{N}(0, (t - s)Q)$  for all  $0 \leq s \leq t$ .

In analogy to the Karhunen–Loève expansion, it can be shown that  $W(t)$  is a  $Q$ -Wiener process if and only if for all  $t \geq 0$ ,

$$W(t) = \sum_{j=1}^{\infty} \sqrt{\lambda_j} \phi_j \beta_j(t),$$

where  $\beta_j(t)$  are i.i.d. Brownian motions, and the series converges in  $L^2(\Omega, H)$ . Moreover, the series is  $\mathbb{P}$ -a.s. uniformly convergent on  $[0, T]$  for arbitrary  $T > 0$  (i.e., converges in  $L^2(\Omega, C([0, T], H))$ ). One should note that formally if we let  $Q = I$ ,  $Q$ -Wiener process becomes cylindrical Wiener process which converges in a larger space.

In dimension 1, we set the domain  $D = (0, L)$  and consider an  $H_{per}^r(D)$ -valued  $Q$ -Wiener process  $W(t)$ , for a given  $r \geq 0$ . (In the KdV case, we take  $r = 2$ .) We take the ONB  $\phi_k(x) = \sqrt{2/L} \sin(k\pi x/L)$  with corresponding  $\lambda_j = (\lfloor j/2 \rfloor + 1)^{-(2r+1+\epsilon)}$  for an  $\epsilon > 0$  (we take  $\epsilon = 0.001$ ), and sample from the truncated expansion  $W^J(t) = \sum_{j=1}^J \phi_j \beta_j(t)$  at the points  $x_k = kL/N$  for  $k = 1, \dots, N$ .

In dimension 2, we set  $D = (0, L_x) \times (0, L_y)$ , take the  $L^2(D)$ -ONB  $\phi_{j,k}(x, y) = 1/\sqrt{L_x L_y} e^{2i\pi(jx/L_1 + ky/L_2)}$  with corresponding  $\lambda_{j,k} = e^{-\alpha(j^2+k^2)}$ , for a parameter  $\alpha > 0$ . (In the NSE case, we take  $\alpha = 0.005$ .) Then we sample from the truncations  $W^{J_x, J_y}(t) = \sum_{j=-J_x/2+1}^{J_x/2} \sum_{k=-J_y/2+1}^{J_y/2} \sqrt{\lambda_{j,k}} \phi_{j,k} \beta_{j,k}(t)$  at  $x_m = mL_x/N_x$ ,  $y_n = nL_y/N_y$  for  $m = 1, \dots, N_x$ ;  $n = 1, \dots, N_y$ .

### A.3 The ill-posedness of the dynamic $\Phi_2^4$ model

We begin with the definition of Hölder–Besov space. Let  $\chi, \theta$  be nonnegative radial functions on  $\mathbb{R}^d$ , such that

- i.  $\text{supp}(\chi)$ , the support of  $\chi$ , is contained in a ball and the support of  $\theta$  is contained in an annulus;
- ii.  $\chi(z) + \sum_{j \geq 0} \theta(2^{-j}z) = 1$  for all  $z \in \mathbb{R}^d$ ;
- iii.  $\text{supp}(\chi) \cap \text{supp}(\theta(2^{-j}\cdot)) = \emptyset$  for  $j \geq 1$  and  $\text{supp}(\theta(2^{-i}\cdot)) \cap \text{supp}(\theta(2^{-j}\cdot)) = \emptyset$  for  $|i-j| > 1$ .

We call such  $(\chi, \theta)$  a dyadic partition of unity, for whose existence we refer to [1, Proposition 2.10]. Let  $\mathcal{F}$  be the Fourier operator, the Littlewood–Paley blocks are now defined as

$$\Delta_{-1}u = \mathcal{F}^{-1}(\chi \mathcal{F}u) \quad \Delta_j u = \mathcal{F}^{-1}(\theta(2^{-j}\cdot) \mathcal{F}u).$$

For  $\alpha \in \mathbb{R}$ ,  $p, q \in [1, \infty]$ , we define

$$\|u\|_{B_{p,q}^\alpha} := \left( \sum_{j \geq -1} (2^{j\alpha} \|\Delta_j u\|_{L^p})^q \right)^{1/q},$$

with the usual interpretation as  $L^\infty$  norm in case  $q = \infty$ . The Besov space  $B_{p,q}^\alpha$  consists of the completion of smooth functions with respect to this norm and the Hölder–Besov space  $\mathcal{C}^\alpha$  is given by  $\mathcal{C}^\alpha = B_{\infty,\infty}^\alpha$ . We point out that everything above can be applied to distributions on the torus considering periodic spaces. For  $\alpha > 0$ ,  $\mathcal{C}^\alpha$  is equivalent to Hölder space. See [17] for details.

In the case of dynamical  $\Phi_2^4$  model, the space-time white noise  $\xi \in \mathcal{C}^{-2-\alpha}(\forall \alpha > 0)$  [8]. The equation now falls in the subcritical regime in the language of Hairer’s regularity structures theory. This means the regularity of solution  $u$  is the same as the regularity of the stochastic convolution  $X$ , the model can be understood as a perturbation of the solution to the linear equation. By standard Schauder’s estimates in the elliptic PDE theory,  $u$  and  $X$  are expected to take values in space  $\mathcal{C}^{-\alpha}(\forall \alpha > 0)$ , which means  $u$  is not a function but a distribution and leaves the non-linear term  $u^3$  undefined in the classical sense. See [8, 5] for details.

## B Additional demo for users

**Data Format:** Datasets are stored in PARQUET format. File naming format is {SPDE name}-{Tasks}-{Truncation degree}-{Sample size}.parquet. For the KdV equation, different noise generated by  $Q$ -Wiener process and Cylindrical Wiener process are denoted by  $Q$  and *cyl*.

```

from SPDE_HACKATHON.model.NSPDE.utilities import *
parquetfile = ".../Phi42+expl_xi_eps_2_1200.parquet"
data_path = ".../Phi42"
get_data_Phi42(parquetfile, data_path)
data = scipy.io.loadmat("../Phi42mat_data.mat")
W, Sol = data['W'], data['sol']
xi = torch.from_numpy(W.astype(np.float32))
data = torch.from_numpy(Sol.astype(np.float32))
train_loader, test_loader = dataloader_nspde_2d(data, xi, ntrain, ntest, T,
sub_t, sub_x, batch_size)

```

Listing 2: Using the Pytorch data loader

For the  $\Phi_1^4$  equation, different value of the parameter  $\sigma$  are denoted by *01* and *1*. For the  $\Phi_2^4$  equation, data generated with renormalization and without renormalization are denoted by *reno* and *expl*.

## C Experimental details

For all experiments, the dataset is split into training, validation and test sets with relative sizes 70%/15%/15%. We use the validation set for hyperparameter tuning and early stopping. For each model and each SPDE dataset with multiple noise truncation degrees, we search the hyperparameters for network training on dataset with one degree ( $J = 128$ ) on the task " $\xi \rightarrow u$ " and apply the best one in other cases. For all the baseline models except DLR-Net, we follow the grid search schemes for hyperparameter selection in [16]; for the DLR-Net, since the numerical-solution setups of our  $\Phi_1^4$  and NSE datasets are similar to what has been experimented in [4], we directly employ their configuration. More details about our experiments (such as the optimizer, scheduler, and the specific values of hyperparameters we used) can be found in our code documentation on Github. We report part of the grid search results in Table 8 and Table 9.

## D Additional experimental results

In this section, we show more experimental results in Table 10 to 14. As the performance of FNO, NSPDE, DLR-Net is significantly better than other models, we mainly evaluate the performance of these three models on KdV, wave equation and incompressible NSE. For DLR-Net, it requires to develop the regularity feature layer for different SPDEs which is beyond the scope of this paper. Therefore, we only apply it on incompressible NSE according to its original work [4]. For the incompressible NSE, in the task  $\xi \mapsto u$ , the initial condition is sampled from  $\mathcal{N}(0, 3^2(-\Delta + 9I)^{-3})$  and fixed. In the task  $(u_0, \xi) \mapsto u$ , the initial condition is  $w^* + w_0$ , where  $w^*$  is sampled from  $\mathcal{N}(0, 3^2(-\Delta + 9I)^{-3})$  and fixed and  $w_0 \sim \mathcal{N}(0, 3^2(-\Delta + 9I)^{-3})$ . Figure 3 illustrates the prediction results from one of the experiments on NSE. Moreover, we generate 500 additional samples in the case of NSE( $J = 256$ ) and test the pre-trained models on them to evaluate the model loss error. Results are reported in Table 14.

Table 8: Grid search NSPDE ( $\Phi_2^4$ ,  $\mathcal{D}_{128}^{\text{re}}$ )

| $d_h$ | Picard's iterations | modes 1 | modes 2 | modes 3 | # Para  | validation loss |
|-------|---------------------|---------|---------|---------|---------|-----------------|
| 32    | 1                   | 8       | 8       | 8       | 530945  | 0.249           |
| 32    | 2                   | 8       | 8       | 8       | 530945  | 0.249           |
| 32    | 3                   | 8       | 8       | 8       | 530945  | 0.249           |
| 32    | 4                   | 8       | 8       | 8       | 530945  | 0.251           |
| 32    | 1                   | 8       | 16      | 8       | 1055233 | 0.238           |
| 32    | 2                   | 8       | 16      | 8       | 1055233 | 0.239           |
| 32    | 3                   | 8       | 16      | 8       | 1055233 | 0.239           |
| 32    | 4                   | 8       | 16      | 8       | 1055233 | 0.239           |
| 32    | 1                   | 16      | 8       | 8       | 1055233 | 0.238           |
| 32    | 2                   | 16      | 8       | 8       | 1055233 | 0.235           |
| 32    | 3                   | 16      | 8       | 8       | 1055233 | 0.237           |
| 32    | 4                   | 16      | 8       | 8       | 1055233 | 0.238           |
| 32    | 1                   | 16      | 16      | 8       | 2103809 | 0.239           |
| 32    | 2                   | 16      | 16      | 8       | 2103809 | 0.238           |
| 32    | 3                   | 16      | 16      | 8       | 2103809 | 0.239           |
| 32    | 4                   | 16      | 16      | 8       | 2103809 | 0.238           |

Table 10: Relative  $L^2$ -error on the test set of KdV. Data is generated with different truncation degrees ( $J=32 \mid 64 \mid 128 \mid 256$ ). ( $\xi$  is sampled from a cylindrical Wiener process and  $\sigma = 0.5$ )

| Model | $\xi \mapsto u$ |       |       |       | $(u_0, \xi) \mapsto u$ |       |       |       |
|-------|-----------------|-------|-------|-------|------------------------|-------|-------|-------|
|       | $J=32$          | 64    | 128   | 256   | $J=32$                 | 64    | 128   | 256   |
| FNO   | 0.072           | 0.071 | 0.118 | 0.166 | x                      |       |       |       |
| NSPDE | 0.010           | 0.012 | 0.093 | 0.134 | 0.013                  | 0.015 | 0.090 | 0.126 |

Table 11: Relative  $L^2$ -error on the test set of the KdV Equation. Data is generated with different truncation degrees ( $J=32 \mid 64 \mid 128 \mid 256$ ). ( $\xi$  is sampled from a  $Q$ -Wiener process and  $\sigma = 1$ )

| Model | $\xi \mapsto u$ |       |       |       | $(u_0, \xi) \mapsto u$ |       |       |       |
|-------|-----------------|-------|-------|-------|------------------------|-------|-------|-------|
|       | $J=32$          | 64    | 128   | 256   | $J=32$                 | 64    | 128   | 256   |
| FNO   | 0.045           | 0.047 | 0.046 | 0.048 | x                      |       |       |       |
| NSPDE | 0.006           | 0.006 | 0.006 | 0.006 | 0.009                  | 0.009 | 0.008 | 0.008 |

Table 12: Relative  $L^2$ -error on the test set of the wave Equation. Data is generated with different truncation degrees ( $J=32 \mid 64 \mid 128 \mid 256$ ).

| Model | $\xi \mapsto u$ |       |       |       | $(u_0, \xi) \mapsto u$ |       |       |       |
|-------|-----------------|-------|-------|-------|------------------------|-------|-------|-------|
|       | $J=32$          | 64    | 128   | 256   | $J=32$                 | 64    | 128   | 256   |
| FNO   | 0.009           | 0.011 | 0.016 | 0.026 | x                      |       |       |       |
| NSPDE | 0.007           | 0.008 | 0.014 | 0.021 | 0.006                  | 0.007 | 0.018 | 0.024 |

Table 9: Grid search NSPDE-S ( $\Phi_2^4$ :  $\mathcal{D}_{128}^{\text{re}}$ )

| $d_h$ | Picard's iterations | modes 1 | modes 2 | modes 3 | # Para  | validation loss |
|-------|---------------------|---------|---------|---------|---------|-----------------|
| 32    | 1                   | 8       | 8       | 8       | 530945  | 0.030           |
| 32    | 2                   | 8       | 8       | 8       | 530945  | 0.024           |
| 32    | 3                   | 8       | 8       | 8       | 530945  | 0.028           |
| 32    | 4                   | 8       | 8       | 8       | 530945  | 0.028           |
| 32    | 1                   | 8       | 16      | 8       | 1055233 | 0.022           |
| 32    | 2                   | 8       | 16      | 8       | 1055233 | 0.021           |
| 32    | 3                   | 8       | 16      | 8       | 1055233 | 0.018           |
| 32    | 4                   | 8       | 16      | 8       | 1055233 | 0.025           |
| 32    | 1                   | 16      | 8       | 8       | 1055233 | 0.020           |
| 32    | 2                   | 16      | 8       | 8       | 1055233 | 0.021           |
| 32    | 3                   | 16      | 8       | 8       | 1055233 | 0.025           |
| 32    | 4                   | 16      | 8       | 8       | 1055233 | 0.025           |
| 32    | 1                   | 16      | 16      | 8       | 2103809 | 0.014           |
| 32    | 2                   | 16      | 16      | 8       | 2103809 | 0.016           |
| 32    | 3                   | 16      | 16      | 8       | 2103809 | 0.021           |
| 32    | 4                   | 16      | 16      | 8       | 2103809 | 0.028           |

Table 13: Relative  $L^2$ -error on the test set of the Navier–Stokes (vorticity) Equation. Data is generated with different truncation degrees ( $J=32 \mid 64 \mid 128 \mid 256$ ). The resolution for training and test data are  $16 \times 16$ .

| Model | $\xi \mapsto u$ |       |       |       | $(u_0, \xi) \mapsto u$ |       |       |       |
|-------|-----------------|-------|-------|-------|------------------------|-------|-------|-------|
|       | $J=32$          | 64    | 128   | 256   | $J=32$                 | 64    | 128   | 256   |
| FNO   | 0.092           | 0.090 | 0.090 | 0.090 | x                      |       |       |       |
| NSPDE | 0.037           | 0.038 | 0.037 | 0.037 | 0.072                  | 0.053 | 0.066 | 0.063 |
| DLR   | 0.023           | 0.023 | 0.023 | 0.022 | 0.022                  | 0.033 | 0.021 | 0.026 |

Table 14: Statistics (mean  $\pm$  standard deviation) of pre-trained models' prediction loss evaluated on an additionally generated NSE( $J = 256$ ) test set of 500 samples

| Model | $\xi \mapsto u$   | $(u_0, \xi) \mapsto u$ |
|-------|-------------------|------------------------|
| FNO   | $0.090 \pm 0.007$ | x                      |
| NSPDE | $0.038 \pm 0.003$ | $0.061 \pm 0.026$      |
| DLR   | $0.023 \pm 0.002$ | $0.026 \pm 0.007$      |

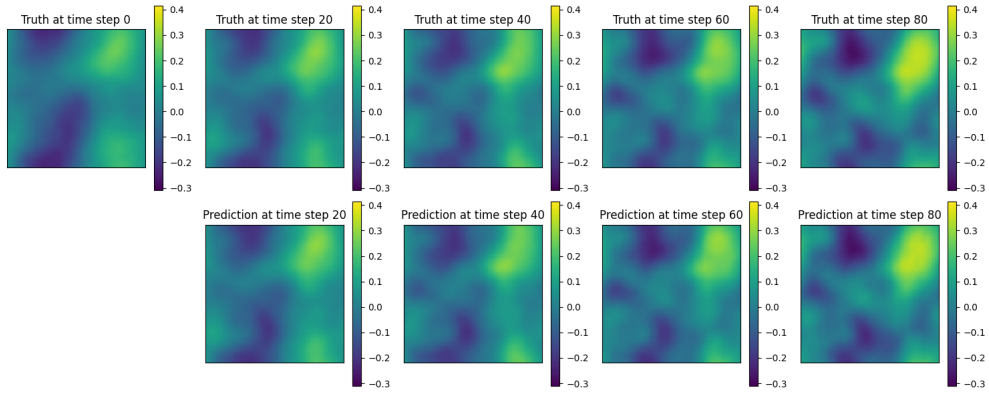


Figure 3: Illustration of the time evolution of the NSE( $J=256$ ) data and NSPDE's predictions. The model is trained on a  $16 \times 16$  mesh and evaluated on a  $64 \times 64$  mesh for visualization. **Top panel:** Ground truth generated by the numerical solver. **Bottom panel:** Predictions from the model with input  $(u_0, \xi)$ .